BIOCHEMISTRY
including biophysical chemistry & molecular biology

Article

pubs.acs.org/biochemistry

Membrane-Perturbing Properties of Two Arg-Rich Paddle Domains from Voltage-Gated Sensors in the KvAP and HsapBK K^+ Channels

Sofia Unnerståle, Fatemeh Madani, Astrid Gräslund, and Lena Mäler*

Department of Biochemistry and Biophysics, The Arrhenius laboratory, Stockholm University, 10691 Stockholm, Sweden

ABSTRACT: Voltage-gated K^+ channels are gated by displacement of basic residues located in the S4 helix that together with a part of the S3 helix, S3b, forms a "paddle" domain, whose position is altered by changes in the membrane potential modulating the open probability of the channel. Here, interactions between two paddle domains, KvAPp from the K_v channel from *Aeropyrum pernix* and HsapBKp from the BK channel from *Homo sapiens*, and membrane models have been studied by spectroscopy. We show that both paddle domains induce calcein leakage in large unilamellar vesicles, and we suggest that this leakage represents a general thinning of the bilayer, making movement of the whole paddle domain plausible. The fact that HsapBKp induces more leakage than KvAPp may be explained by the presence of a Trp residue in HsapBKp. Trp residues generally promote localization to the hydrophilic−hydrophobic interface and disturb tight packing. In magnetically aligned bicelles, KvAPp increases the level of order along the whole acyl chain, while HsapBKp affects the morphology, also indicating that KvAPp adapts more to the lipid environment. Nuclear magnetic resonance (NMR) relaxation measurements for HsapBKp show that overall the sequence has anisotropic motions. The S4 helix is well-structured with restricted local motion, while the turn between S4 and S3b is more flexible and undergoes slow local motion. Our results indicate that the calcein leakage is related to the flexibility in this turn region. A possibility by which HsapBKp can undergo structural transitions is also shown by relaxation NMR, which may be important for the gating mechanism.

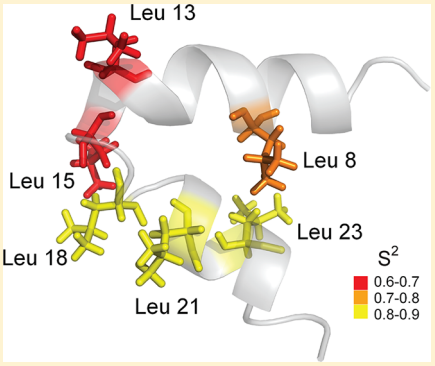

Voltage-gated K^+ channels, K_v channels, are gated by charged amino acid residues (Arg or Lys), whose positions are altered by changes in the membrane potential.[1,2] This modulates the probability of the channel being in the open state. The gating charges are found in the S4 transmembrane segment of the voltage-sensing domain (VSD). The S4 helix forms, together with a part of the S3 helix, S3b, a domain known as the "paddle" domain or the "arginine-rich paddle".[2−4] The first structure of a full-length K_v channel revealed that the arginine-rich paddle forms a helix−turn−helix structure situated within the hydrocarbon core of the membrane.[2,3] This positioning is controversial, because of the great hydrophilicity of arginine. Many experimental[5−7] and theoretical studies[8−10] have aimed to improve our understanding of the molecular basis for the positioning of the Arg-rich paddle. It has been argued that the S4 helix in the paddle motif is fairly independent of the rest of the VSD, and that the structure of this helix is governed by protein−lipid interaction.[11] It has also been demonstrated that the voltage sensor motif can function on its own as a voltage-activated proton channel without a separate pore domain[12,13] and that the paddle domains in K_v and Na_v channels are modular and can be swapped between different ion channels.[14−16] Several studies of isolated paddle domains or of the S4 helix alone have been conducted to shed light on the interaction between this Arg-rich sequence and the lipid bilayer.[11,17] Other studies have shown that the S4 helix alone from the K_v channel KvAP (from the thermophilic archaebacteria *Aeropyrum pernix*)[2,3,6] has properties that resemble those of the intact VSD.[11,17] Despite several studies of VSDs over the past 10 years, the question of whether a change in the membrane potential induces a small charge movement, which rotates and tilts the S4 transmembrane segment,[1] or a larger charge movement, which alters the position of the whole paddle domain (S3b−S4),[2] is still being debated. A third possibility is that the thickness of the lipid bilayer is significantly reduced by the paddle domain because of hydrophobic mismatch, which means that the movement does not need to be that large.[8,9,18]

The aim of this study was to investigate how paddle domains from two different channels, the K_v channel KvAP (from *A. pernix*, GI|14601099)[2,3,6] and the BK channel HsapBK (from *Homo sapiens*, GI|2570854),[19] interact with membranes to be able to draw general conclusions about the mechanism of gating and to be able to compare paddle domains from two different subtypes. We have previously determined the high-resolution NMR structure of the paddle domain from HsapBK [HsapBKp, corresponding to HsapBK(233−260)] in DPC micelles.[19] The solution structure revealed a helix−turn−helix structure similar to the structure of the corresponding sequence in KvAP as determined by X-ray crystallography.[2,3,19] In this study, the interactions between the paddle domains from KvAP [KvAPp, corresponding to KvAP(112−146)] and from HsapBK (HsapBKp) and lipids were studied by fluorescence, circular dichroism (CD), and NMR spectroscopy. To investigate bilayer perturbation induced by the paddle domains,

Received: February 10, 2012
Revised: April 25, 2012
Published: April 25, 2012

Table 1. Primary Structures of the Paddle Domains and of Selected CPPs

peptide	% Arg	% Trp	total charge	average hydrophobicity[a]	sequence
KvAPp	14	0	+4	0.40	PAGLLALIEGHLAGLGLFRLVRLLRFLRILLIISR
HsapBKp	14	1	+3	0.65	PVFVSVYLNRSWLGLRFLRALRLIQFSE
M918	32	0	+7	0.93	MVTVLFRRLRIRRASGPPRVRV
mPrPp	4	2	+3	0.74	MANLGYWLLALFVTMWTDVGLCKKRPKP
bPrPp	3	2	+5	0.80	MVKSKIGSWILVLFVAMWSDVGLCKKRPKP

[a]The average hydrophobicity was calculated utilizing the von Heijne scale for biological hydrophobicity.[65]

leakage of the fluorophore calcein from large unilamellar vesicles (LUVs) was monitored by fluorescence spectroscopy.[20−23] Circular dichroism was used to examine the lipid-dependent structure induction, while deuterium NMR spectra of acyl chain deuterated DMPC and DMPG in magnetically aligned bicelles were acquired to investigate the effects of the paddle domains on bilayer order and integrity. The dynamics of selectively ^{15}N-labeled HsapBKp in DPC micelles or 9:1 DPC/DPG micelles was also investigated by ^{15}N spin relaxation under the same conditions that were used for the solution structure.

Many natural and synthetic membrane-interacting peptides, such as cell-penetrating peptides (CPPs), i.e., peptides that can transport biological therapeutics into cells, antimicrobial peptides, and toxins contain a large number of basic residues but are still able to interact with bilayers, causing membrane perturbation and even translocation through a bilayer.[24−31] CPPs are characterized by this high Arg content together with a great average hydrophobicity,[25,32,33] which are properties shared by the paddle domains (Table 1). A general understanding of the influence of hydrophobicity and basic amino acid residues on membrane properties is therefore of great interest. Hence, we have compared our results for the paddle domains with results for other Arg-containing peptides: the cell-penetrating peptide M918[34] and the N-terminal fragments of mouse (mPrPp) and bovine prion protein (bPrPp).[35] The results are thus important for understanding the role of the basic amino acid residues in membrane interactions in general, as well as for understanding how these paddle domains in the intact potassium channels may influence the lipid bilayer.

EXPERIMENTAL PROCEDURES

Materials. Synthetic peptides corresponding to either HsapBK(233−260) or KvAP(112−146), including fluorescein-labeled βAla-KvAPp and ^{15}N-Leu-labeled HsapBKp, were obtained from PolyPeptide Group (Strasbourg, France) and used without further purification. Calcein, a fluorescein derivative ($C_{30}H_{26}N_2O_{13}$, 622.5 Da), was obtained from Molecular Probes (The Netherlands).

1-Palmitoyl-2-oleoyl-*sn*-glycero-3-phosphocholine (POPC) and 1-palmitoyl-2-oleoyl-*sn*-glycero-3-phospho-(1′-*rac*-glycerol) (POPG) were used to produce large unilamellar vesicles (LUVs). 1,2-Dihexanoyl-d_{22}-*sn*-glycero-3-phosphocholine (DHPC) was used as the short chain phospholipid in the phospholipid bicelles. Both deuturated (d_{54}) and undeuturated 1,2-dimyristoyl-*sn*-glycero-3-phosphocholine (DMPC) and 1,2-dimyristoyl-*sn*-glycero-3-phospho-(1′-*rac*-glycerol) (DMPG) were used in different samples to produce the bilayer in phospholipid bicelles. All lipids were obtained from Avanti Polar Lipids (Alabaster, AL). The detergent d_{38}-dodecylphosphocholine (DPC) was obtained from Cambridge Isotope Laboratories (Andover, MA), dodecyl-phospho-*rac*-glycerol sodium salt (DPG) from Alexis (Switzerland), and Triton X-100 from Sigma-Aldrich (Stockholm, Sweden).

Preparation of Large Unilamellar Vesicles. LUVs with a diameter of 100 nm were used for calcein leakage experiments and CD measurements. To produce zwitterionic and 30% negatively charged LUVs, POPC or a 7:3 POPC/POPG mixture was initially dissolved in chloroform to obtain homogeneous solutions. The solvent was then removed by evaporation under high vacuum for 3 h. The resulting dried lipid films were subsequently resuspended in phosphate buffer (pH 7.2) and vortexed for 10 min to obtain a more defined size distribution. These solutions were then subjected to five freeze−thaw cycles to decrease lamellarity. Finally, to obtain uniform LUVs, the samples were extruded using an Avanti manual extruder approximately 20 times through a polycarbonate microfilter with a pore size of 100 nm.[36]

Release of Calcein from Large Unilamellar Vesicles. For the calcein leakage experiments, LUVs were prepared as described above. The buffer was a 50 mM potassium phosphate buffer (pH 7.2) with 55 mM calcein dissolved. Calcein not entrapped inside the LUVs was removed by filtration through Sephadex-G25 columns two times. The fluorescence intensity of calcein should be low because of self-quenching and increase upon dilution. After the background intensity had been measured, KvAPp or HsapBKp was titrated to either 0.1 mM POPC or a 0.1 mM POPC/POPG mixture (7:3) at 25 °C, from a 0.67 mM stock solution in a 2:1 ddH_2O/methanol mixture, yielding concentrations of 5 and 10 μM. The methanol was added because of the low solubility of the paddle domains in buffer, and as a control, methanol was added to LUVs to make sure that this did not influence the leakage. The release of calcein from the vesicles, as a consequence of adding the paddle domains, was monitored over 10 min as an increase in fluorescence intensity using a Horiba Jobin Yvon Fluorolog-3 spectrofluorometer with wavelengths set at 490 nm for excitation and 516 nm for emission. The background fluorescence, F_0, was used as a measure of 0% leakage. In the final step, 100% leakage, i.e., destruction of the vesicles, was induced by addition of 10% (w/v) Triton X-100, giving an upper reference level of fluorescence, F_r. The degree of leakage induced by the paddle domains was then calculated using the following equation:

$$\%\,\text{leakage} = (F - F_0)/(F_r - F_0) \times 100 \quad (1)$$

where F is the fluorescence intensity in the presence of KvAPp or HsapBKp. The experiments were performed three times, and the same trend was seen in all cases.

Circular Dichroism Spectroscopy. CD samples with a concentration of 0.1 mM POPC or POPC/POPG mixture (7:3) and a potassium phosphate buffer concentration of 50 mM (pH 7.2) were prepared as described above. The low concentration of LUVs was chosen to diminish disturbances due to light scattering. The paddle domains were titrated to these solutions from 0.67 mM stock solutions in a 2:1 ddH_2O/methanol mixture, yielding concentrations between 5 and 55 μM, and spectra were acquired. In this way, the methanol content in the final sample was kept to a minimum. In addition, CD spectra of 48 μM KvAPp and HsapBKp in 48 mM DPC

dx.doi.org/10.1021/bi300188t | Biochemistry 2012, 51, 3982−3992

micelles in 50 mM sodium phosphate buffer (pH 7.2) were acquired and compared to spectra for samples to which methanol had been added, yielding a 2:1 buffer/methanol solution, to make sure that methanol had no effect on structure induction.

The far-UV CD spectra were acquired on a Chirascan CD spectrometer using a 2 mm quartz cell. The temperature was maintained at 25 °C with a TC 125 temperature controller. Wavelengths ranging from 190 to 260 nm were measured with a 0.5 nm step resolution. Spectra were collected and averaged over 10 measurements. Background spectra of vesicles or micelles without the paddle domains were subtracted. To estimate the percentage of different secondary structures in the CD spectra, we utilized the CDSSTR method[37−39] in DICHROWEB[40] using reference set 7 optimized for 190−240 nm.

Deuterium NMR of Magnetically Partially Oriented Lipid Bilayers. Magnetically aligned phospholipid bicelles with a total lipid concentration of 300 mM and a q of 3.5 were prepared. The bilayer-forming part consisted of DMPC-d_{54}, a 7:3 DMPC-d_{54}/DMPG mixture, or a 7:3 DMPC/DMPG-d_{54} mixture. These lipids were vortexed in 50 mM sodium phosphate buffer (pH 7.2) to yield uniform slurries; 66 mM DHPC was then added to all solutions, which were vortexed again and stored at 4 °C overnight. To produce clear solutions, the samples were subjected to cooling and heating cycles between 4 and 50 °C. Background spectra of all three bicelle samples were measured. KvAPp or HsapBKp (1 mM) in a 2:1 ddH_2O/methanol mixture was then added to the samples, which were subsequently lyophilized to remove the methanol. The lipid films created in this way were dissolved in ddH_2O, incubated at 4 °C, subjected to new heating and cooling cycles (between 4 and 40 °C), and vortexed until all lipids were dissolved.

Deuterium experiments were performed at a ^{2}H frequency of 61.4 MHz (9.4 T) using a Bruker Avance spectrometer equipped with a tunable broad-band probe. All NMR samples were incubated in the spectrometer, first at 15 °C for 15 min yielding an isotropic solution and then at 37 °C for 30 min yielding magnetically aligned bicelles, before spectra were recorded; 37 °C is well above the gel−liquid crystal phase transition temperature, which is 24 °C for DMPC and 20.5 °C for DMPC-d_{54},[41] assuring that the bicelles are in the lamellar liquid crystalline state, L_α. Standard quadrupolar delay spectra $(\pi/2-\tau_1-\pi/2-\tau_2-\text{acq})$ were acquired for both bicelle solutions with and without peptides, using a $\pi/2$ pulse width of 14 μs, and with the delays set to 50 μs (τ_1) and 48 μs (τ_2); 1024 scans were measured and averaged, and a 2 s delay was used between scans. The FID was multiplied with an exponential line broadening function prior to Fourier transformation.

Quadrupolar splittings ($\Delta\nu_q$) were measured in the spectra. In concentrated DMPC/DHPC mixtures well above the gel−L_α transition temperature, the dominating bilayer species is aligned with its normal perpendicular to the static magnetic field, yielding the following relation between $\Delta\nu_q$ and the order parameter, S_{CD}:

$$\Delta\nu_q = \frac{3}{4}\left(\frac{e^2qQ}{h}\right)S_{CD} \qquad (2)$$

where $(e^2qQ)/h$ is the quadrupolar coupling constant for a C−D bond (167 kHz).[42,43] Because the quadrupolar splitting ($\Delta\nu_q$) is related to the segmental order parameter, S_{CD}, an increase in $\Delta\nu_q$ is generally associated with an increase in the level of order of the system, while a decrease in $\Delta\nu_q$ is associated with a decrease in the level of order.

Dynamics Studied by ^{15}N Spin Relaxation. ^{15}N−[^{1}H] longitudinal (T_1) and transverse (T_2) relaxation times and heteronuclear NOEs were measured for [^{15}N]Leu-labeled HsapBKp (Leu8, Leu13, Leu15, Leu18, Leu21, and Leu23) in DPC and 9:1 DPC/DPG micelles in a 10% ^2H_2O/90% 50 mM sodium phosphate buffer mixture (pH 7.2). In DPC, the paddle domain concentrations were 500 μM and 1 mM and the DPC concentrations were 50 and 100 mM, respectively. In the DPC/DPG sample, the peptide concentration was 200 μM and the detergent concentration was 20 mM, keeping the P:L ratio constant in all measurements. The experiments were conducted using Bruker Avance spectrometers at 16.4, 14.1, and 11.7 T. R_1 NOE and R_2 ^{15}N relaxation parameters were determined using standard sensitivity-enhanced pulse sequences.[44,45] Further, a three-dimensional edited ^{15}N−H NOESY-HSQC spectrum was acquired at 11.7 T for ^{15}N shift assignment purposes. All experiments were conducted at 37 °C. The T_1 relaxation was determined from the following series of relaxation delays: 10, 30, 60, 100, 150, 300, 500, 700, 1000, 1400, 2000, and 2500 ms. The T_2 relaxation was measured using CPMG delays of 16, 32, 80, 95, 143, 190, and 238 ms. Two of the T_1 and T_2 experiments were repeated to estimate the error that was set to 0.1 for R_1 and 1 for R_2. All spectra were evaluated using Topspin (version 3.0). Single-exponential decays were fit using GraFit version 3.09b. Heteronuclear NOEs were calculated by dividing the intensity of the ^{15}N−H peaks in a NOE-enhanced spectrum by the corresponding intensities in the unsaturated spectrum. Errors of 10% were used for the NOE values. The relaxation data were subsequently analyzed with Modelfree 4.15[46,47] to yield the motional parameters using the Lipari−Szabo model-free approach.[48,49]

RESULTS

Calcein Leakage Induced by the Paddle Domains. The effect of the concentration of the two paddle domains, KvAPp and HsapBKp, on the induced leakage from LUVs composed of either zwitterionic lipids (POPC) or a 7:3 mixture of POPC and negatively charged lipids (POPG) was investigated. Figure 1 shows the percent of calcein leakage, calculated according to eq 1, as a function of paddle domain concentration and lipid composition. For POPC LUVs, we see that HsapBKp induces more leakage of calcein than KvAPp at both concentrations

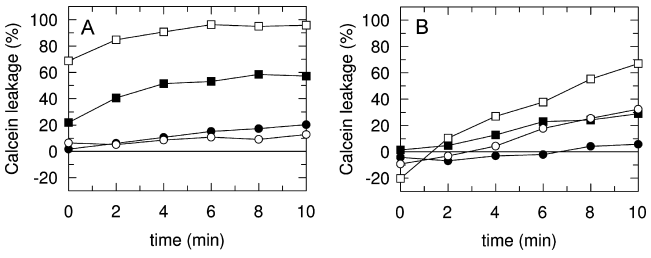

Figure 1. Time-dependent fluorescence signals representing leakage of calcein from LUVs containing 55 mM entrapped calcein at 25 °C and pH 7.2. The effects of KvAPp (circles) and HsapBKp (squares) on LUVs composed of (A) 0.1 mM POPC. and (B) a 7:3 0.1 mM POPC/POPG mixture are shown. Filled symbols represent data for 5 μM peptide and empty symbols data for 10 μM peptide. The zero time point is ∼5 s after the addition of the paddle domain to the LUVs. The apparent negative leakage shown in panel B due to dilution of the sample upon addition of the paddle domain is visible because of the slower kinetics in POPC/POPG LUVs.

dx.doi.org/10.1021/bi300188t | Biochemistry 2012, 51, 3982−3992

Table 2. Summary of Calcein Release and Secondary Structures of the Paddle Domains

		P:L = 0.05 (1:20)			P:L = 0.1 (1:10)		
		secondary structure[a]			secondary structure[a]		
peptide	lipid(s)	α	β	% calcein leakage[b]	α	β	% calcein leakage[b]
KvAPp	POPC	35	16	20	20	22	13
	7:3 POPC/POPG	6	26	6	6	27	32
HsapBKp	POPC	4	37	57	4	33	96
	7:3 POPC/POPG	4	36	29	4	36	67

[a]Estimation of the extent of helix and strand from CD spectra (Figure 2) as calculated by the CDSSTR method[37−39] in DICHROWEB.[40] [b]Calcein release recorded 10 min after addition of KvAPp or HsapBKp to calcein-entrapping POPC or 30% negatively charged POPC/POPG LUVs, respectively.

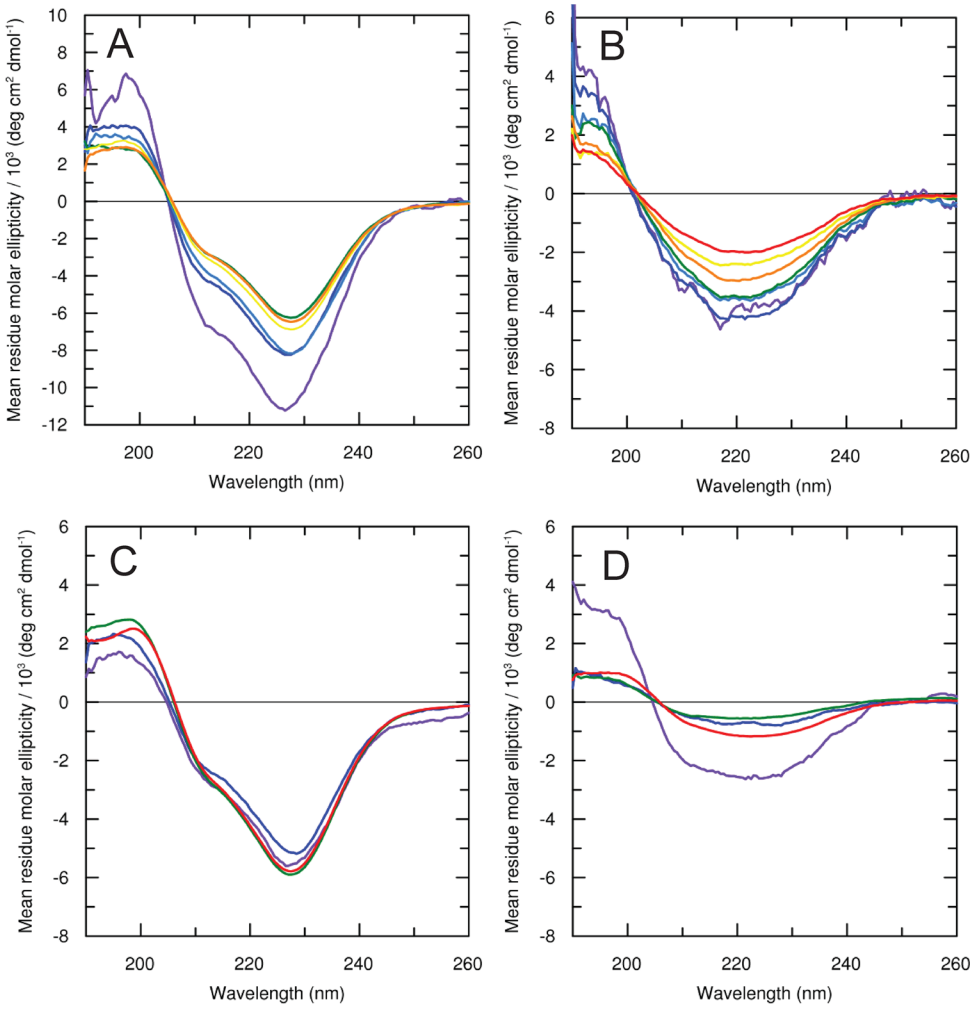

Figure 2. CD spectra recorded for KvAPp (A and C) and HsapBKp (B and D) in 0.1 mM POPC (A and B) or a 7:3 0.1 mM POPC/POPG mixture (C and D) at 25 °C and pH 7.2. For the spectra in POPC, paddle concentrations of 5 μM (purple), 10 μM (blue), 15 μM (light blue), 25 μM (green), 35 μM (yellow), 45 μM (orange), and 55 μM (red) were used, yielding P:L ratios of 1:20, 1:10, 3:20, 1:4, 7:20, 9:20, and 11:20, respectively. For the spectra in the 7:3 POPC/POPG mixture, paddle concentrations of 5 μM (purple), 10 μM (blue), 25 μM (green), and 55 μM (red) were used.

(Figure 1A). Further, the extent of leakage increases with an increased HsapBKp concentration. For POPC/POPG LUVs, HsapBKp still induces more leakage than KvAPp (Figure 1B). Here, the extent of leakage increases with an increased paddle domain concentration for both KvAPp and HsapBKp. When comparing the results in POPC with the results in a 7:3 POPC/POPG mixture, we see that KvAPp shows a similar leakage in both types of vesicles while HsapBKp induces more leakage in POPC (Figure 1 and Table 2). From these results, we conclude that both paddle domains perturb the membrane integrity. However, HsapBKp causes a larger membrane disrupting effect, which is concentration-dependent and appears to be larger in POPC bilayers than in POPC/POPG bilayers.

The Secondary Structure of the Paddle Domains Depends on the Surrounding Lipid Environment. To monitor the induced secondary structure in different membrane mimetics and at different P:L ratios used in this study, CD spectra were acquired. Spectra of KvAPp or HsapBKp (between 5 and 55 μM) in 0.1 mM POPC and a 7:3 0.1 mM POPC/POPG mixture (Figure 2 and Table 2) were measured under

dx.doi.org/10.1021/bi300188t | Biochemistry 2012, 51, 3982−3992

the same conditions that were used in the leakage studies. CD spectra of KvAPp and HsapBKp in DPC micelles were also acquired under the same conditions that were used in the relaxation studies and in the previously determined solution structure.

For KvAPp in POPC, all spectra show minima around 222 nm characteristic of α-helical secondary structure (Figure 2A). However, the 208 nm minimum, characteristic of α-helix, is not so distinct, which indicates that β-structure with a minimum at 215 nm might also be present. Secondary structure estimation using DICHROWEB (Table 2) shows that the helical content is highest and the β-sheet content lowest at the lowest KvAPp concentration (1:20 P:L). When more paddle domain is added, the helical content is decreased and the β-sheet content is increased until a P:L ratio of 1:4 is reached. The spectra for HsapBKp in 0.1 mM POPC are all very similar (Figure 2B) but differ from the spectra of KvAPp. They show a minimum around 215 nm, indicating mainly β-structure, which is confirmed by estimations using DICHROWEB.

The spectra for the paddle domains in a 7:3 POPC/POPG mixture are similar to those in POPC (Figure 2C,D). However, the magnitude of the CD signal is significantly decreased. The low helical content and the high β-sheet content seen at a P:L ratio of 1:4 in POPC have already been reached at a P:L ratio of 1:20. Hence, the β-sheet content can be induced either by introducing charge into the membrane or by elevating the peptide concentration. Estimations of the secondary structure of HsapBKp in 7:3 POPC/POPG LUVs give the same results as in POPC: the dominating secondary structure component is β-strand. A large variation in the relative signal intensity was however observed, indicating that at higher P:L ratios, the peptide aggregates, which results in a loss of the CD signal.

CD measurements for the two paddle domains in DPC (with a peptide:detergent ratio of 1:100) used in the relaxation NMR measurements (Figure 3) were also acquired. CD spectra

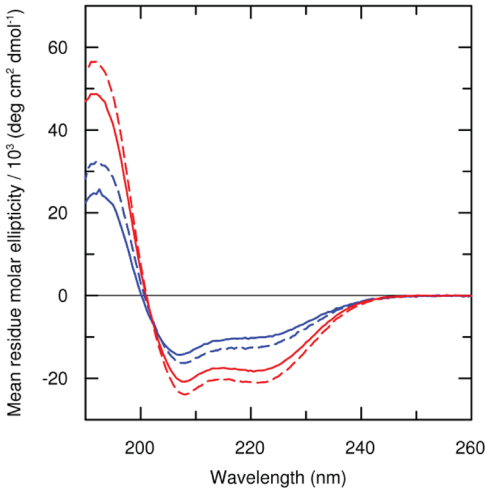

Figure 3. CD spectra of 48 μM KvAPp (red) and HsapBKp (blue) in 48 mM DPC (pH 7.2) (solid lines) or in a 2:1 sodium phosphate buffer/methanol mixture (pH 7.2) (dashed lines) recorded at 25 °C.

of both KvAPp and HsapBKp in DPC micelles showed clear α-helical features, which were very similar to earlier observations in bicelles.[19] Addition of methanol did not affect the secondary structure significantly, suggesting that the methanol added to the LUV samples does not affect the secondary structure significantly either.

In summary, KvAPp has a significant α-helical content in POPC at low peptide concentrations. Via addition of peptide or addition of charge to the LUVs, the amount of β-sheet is increased, while the α-helical contribution decreases. Both types of LUVs induce mainly β-sheet structure in HsapBKp. In micelles at a P:L ratio of 1:100, the paddle domains form helix−turn−helix motifs and thus helical features are seen in the CD spectra. Hence, the structure of these two paddle domains depends critically on the P:L ratio and the features of the surrounding lipid environment.

Deuterium NMR Experiments Show That Both Paddle Domains Affect the Bilayer. To study the influence of the two paddle domains on bilayer order, we recorded ^{2}H quadrupolar spectra at 37 °C for 300 mM magnetically aligned bicelles [q = 3.5 for a DMPC-d_{54}/DHPC, (7:3 DMPC-d_{54}/DMPG)/DHPC, or (7:3 DMPC/DMPG-d_{54})/DHPC mixture] (Figure 4) with and without 1 mM KvAPp or HsapBKp. In panels A and B of Figure 4, deuterated DMPC (DMPC-d_{54}) is monitored, and in Figure 4C, deuterated DMPG (DMPG-d_{54}) is monitored. The magnetically aligned bicelles show typical ^{2}H spectra for the deuterated lipid chains with quadrupolar splittings, $\Delta\nu_q$, for the outermost peaks of DMPC-d_{54} (plateau) of 21 kHz and splittings of the innermost peaks (the methyl deuterons) of 2.4 kHz in both bicelle types. For DMPG-d_{54} in (7:3 DMPC/DMPG)/DHPC bicelles, the corresponding splittings are 20 and 2.4 kHz, respectively (Table 3).

The paddle domains both have small, which is not surprising considering the low P:L ratio (1:300), but significant effects on the ^{2}H spectra. In DMPC bicelles (Figure 4A), KvAPp has a slight ordering effect for all carbons along the acyl chain with an average increase in the splitting, and thus in the order parameter, of 1.6% upon addition of 1 mM KvAPp [when adding 3 mM KvAPp, this increases to 5.2% (data not shown)]. This implies that KvAPp interacts along the whole acyl chain. The effect of HsapBKp on the splittings is more modest.

In 7:3 DMPC/DMPG bicelles, the effect on DMPC-d_{54} (Figure 4B) and DMPG-d_{54} (Figure 4C) was measured separately. KvAPp increased $\Delta\nu_q$ for DMPC-d_{54} by 3.2% on average along the acyl chain and is thus seen to have an ordering effect. This effect is greater in the middle of the acyl chain, with a maximal increase of 4.6% and a minimum when approaching the outermost peak. This indicates that KvAPp is situated in the midpart of the acyl chain farther from the headgroup. HsapBKp, on the other hand, has both modest ordering and disordering effects on DMPC-d_{54}. The main effect, however, is to decrease the peak resolution in the spectrum. This indicates a change in T_2 or a change in mosaic spread, i.e., the distribution of angles relative to B_0, upon addition of the paddle domain. Upon addition of KvAPp to the negatively charged bicelles, the order of DMPG-d_{54} increases only slightly. KvAPp does thus influence DMPC more than DMPG in the DMPC/DMPG bicelles. Addition of HsapBKp causes a decrease in the $\Delta\nu_q$ of DMPG-d_{54} and has thus a disordering effect. The average difference in $\Delta\nu_q$ is −1% with a maximal decrease being −3.4% for position 13 in the acyl chain. Further, the peak resolution is also decreased for DMPG-d_{54}.

The deuterium spectrum of residual HDO was also investigated (Figure 4, right panel). Incomplete averaging of the large ^{2}H quadrupolar splitting (≈16 Hz) caused by rapid exchange between water molecules in the partially aligned hydration shell and in the bulk water creates a doublet spectrum, indicating an ordered bilayer phase.[50,51] KvAPp increases the $\Delta\nu_q$ of the HDO peak in (7:3 DMPC/DMPG)/DHPC bicelles, suggesting an ordering effect. This requires a well-defined peptide−lipid interaction between KvAPp and the bilayer. HsapBKp decreases

dx.doi.org/10.1021/bi300188t | Biochemistry 2012, 51, 3982−3992

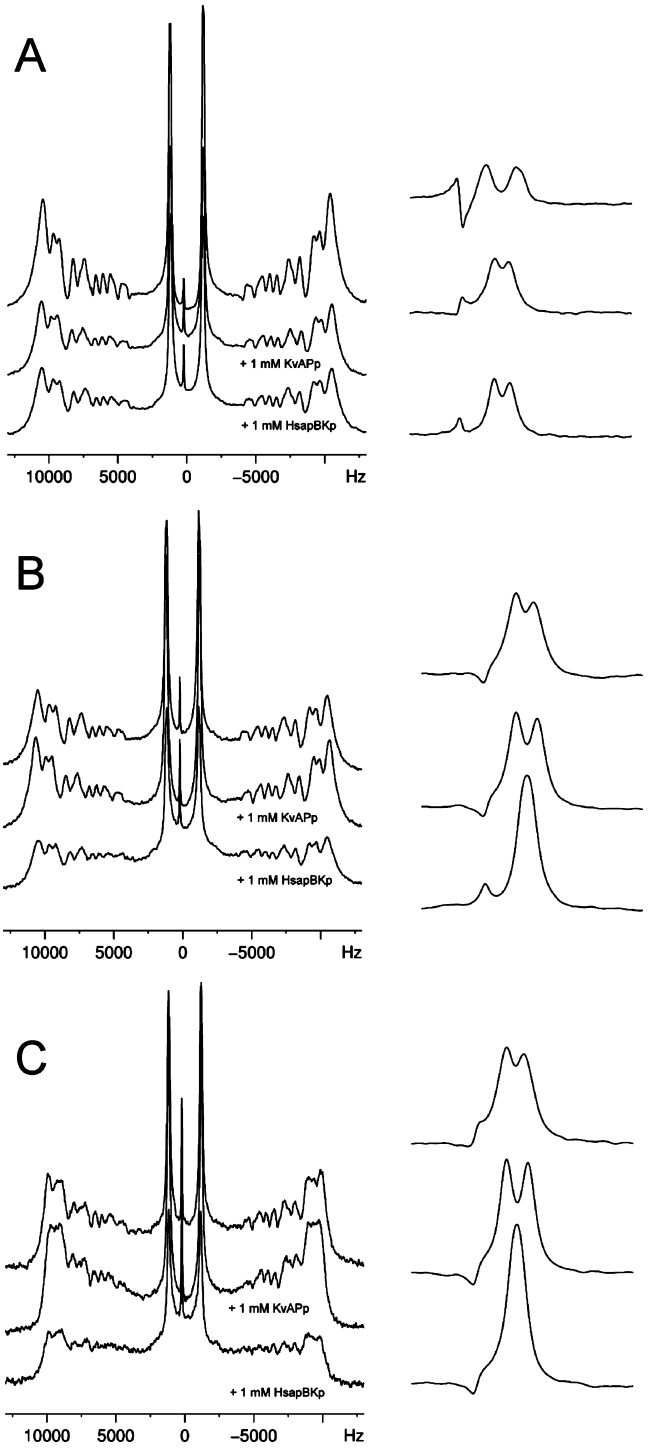

Figure 4. Deuterium NMR spectra of 300 mM DMPC-d_{54}/DHPC bicelles (A), (7:3 DMPC-d_{54}/DMPG)/DHPC bicelles (B), and (7:3 DMPC/DMPG-d_{54})/DHPC bicelles (C) (q = 3.5) at pH 7.2 and 37 °C. The top spectrum is that of bicelles only, the middle spectrum that after the addition of 1 mM KvAPp, and the bottom spectrum that after the addition of 1 mM HsapBKp. The left column shows the spectrum of chain-perdeuturated DMPC or DMPG, while the right column shows the residual HDO signal.

$\Delta\nu_q$ of the HDO peak in (7:3 DMPC/DMPG)/DHPC bicelles (Figure 4B,C, right panel), implying that this paddle domain reduces the order of the bilayer. In DMPC/DHPC bicelles, the HDO signal is not as affected (Figure 4A, right panel). However, a previous study in DMPC/DHPC bicelles using a P:L ratio of

Table 3. Quadrupolar Splittings of DMPC-d_{54} and DMPG-d_{54} in Magnetically Aligned Bicelles at 37 °C

bilayer forming part of the bicelle	plateau $\Delta\nu_p$ (kHz)	difference (%)	methyl $\Delta\nu_m$ (kHz)	difference (%)
DMPC-d_{54}	20.73		2.41	
with KvAPp	21.05	1.5	2.37	−1.8
with HsapBKp	21.07	1.7	2.31	−4.1
DMPC-d_{54}/DMPG	21.00		2.35	
with KvAPp	21.30	1.4	2.42	2.7
with HsapBKp	20.94	−0.3	2.32	−1.7
DMPC/DMPG-d_{54}	19.76		2.36	
with KvAPp	19.35	−2.1	2.38	0.75
with HsapBKp	19.59	−0.9	2.31	−2.1

1:100 shows that at this higher paddle domain concentration the quadrupolar splitting of the HDO peak is smaller.[52] These findings together suggest that HsapBKp interacts stronger with 30% negatively charged bicelles than with zwitterionic bicelles, and the interaction leads to a decrease in bilayer order.

Together, the results indicate that the two paddle domains have opposite effects on the order of the bilayer. KvAPp induces a slight ordering for all carbons along the acyl chain of DMPC in both types of bicelles, while a smaller effect on DMPG is observed. This implies a well-ordered interaction between this paddle domain and the bilayer. HsapBKp, on the other hand, is observed to have very modest effects on the size of the quadrupolar splittings for DMPC, while a decrease in quadrupolar splittings is seen for DMPG. A decrease in peak resolution is seen for both DMPC-d_{54} and DMPG-d_{54} in negatively charged bicelles, indicating that HsapBKp changes the morphology of the phospholipid bicelles.

The Dynamics in HsapBKp Depend on the Lipid Environment. The interaction between HsapBKp and membrane mimetics was further studied by relaxation measurements in DPC as well as in 9:1 DPC/DPG micelles. Studies in bicelles were not feasible because of the excessive line broadening, probably due to strong interaction and/or unfavorable exchange. The six Leu residues (Leu8, Leu13, Leu15, Leu18, Leu21, and Leu23) in HsapBKp were specifically labeled with ^{15}N (Figure 5), and in a ^{15}N-filtered HSQC spectrum, these six

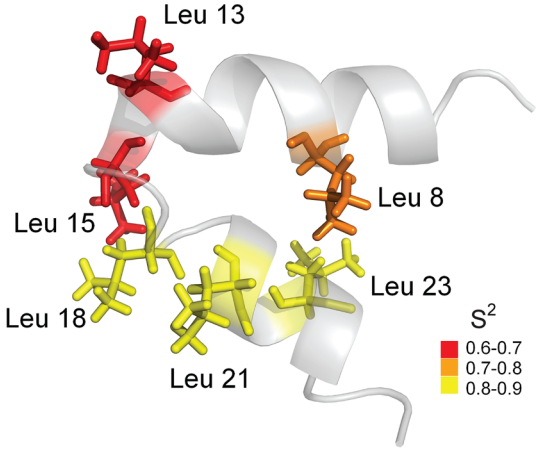

Figure 5. Solution NMR structure of HsapBKp in DPC (Protein Data Bank entry 24kk) with the six Leu residues (Leu8, Leu13, Leu15, Leu18, Leu21, and Leu23) that were specifically labeled with ^{15}N color coded according to their order parameters derived from [^{15}N]Leu-HsapBKp in DPC.

dx.doi.org/10.1021/bi300188t | *Biochemistry* 2012, 51, 3982−3992

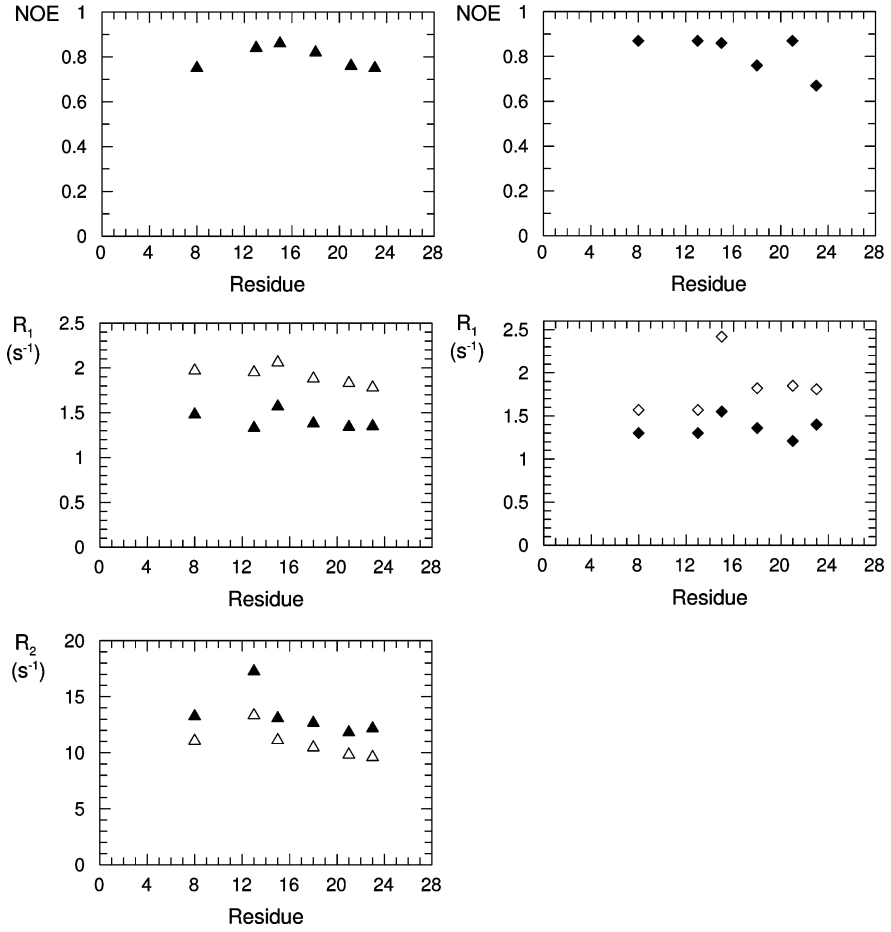

Figure 6. ^{15}N relaxation data for [^{15}N]Leu-HsapBKp in DPC (left) and a 9:1 DPC/DPG mixture (right). Empty triangles are relaxation parameters from measurements at 500 MHz, while filled triangles are from measurements at 700 MHz. In the right panel, filled diamonds are parameters measured at 700 MHz while empty diamonds are R_1 values measured at 600 MHz.

residues gave well-resolved cross-peaks. Assignments for the protons were available from previous investigations,[19] and assignments for the backbone amides were obtained with the aid of a three-dimensional ^{15}N−H NOESY-HSQC spectrum,[44,47,53] which was sufficient because all six Leu residues are preceded by different amino acids. ^{15}N−[^{1}H] longitudinal (T_1) and transverse (T_2) relaxation times as well as heteronuclear NOEs were measured for each Leu residue.

The R_1 ($1/T_1$) rates, the R_2 ($1/T_2$) rates, and the NOEs for HsapBKp in DPC are shown in the left panel of Figure 6. The relaxation parameters are uniform, with one exception, those of Leu13, which is characteristic for a structured globular protein, indicating that HsapBKp indeed is a self-folding domain of its own. Notably, Leu13 has a different R_2 rate than the other residues, suggesting a different dynamic behavior for this residue. Leu13 differs from the others as it has no Arg residue in the vicinity and is situated close to Trp12 and Gly14 in the turn region of the helix−turn−helix motif observed in the solution structure.[19]

The relaxation data were modeled by the model-free approach.[48,49] First, we estimated the overall correlation time for the molecule (τ_M) to be 9.4 ns. Leu13 and Leu18 were excluded from this calculation, because the relaxation data for these residues differed significantly from those of the other four. To see if these differences were a consequence of anisotropic motion, the overall correlation time for each residue was calculated separately by using a spectral density function that included an overall correlation time (τ_{Mi}), a generalized order parameter (S^2), and a local correlation time (τ_{loc}) for the local motion of each ^{15}N−^{1}H bond vector. The overall correlation times for each residue are shown together with the S^2 parameters in Table 4. The large spread in the τ_{Mi} times does indeed indicate that the motion is anisotropic, or the presence of slow local motions that are difficult to separate from the overall motion, making the model-free spectral density function in principle invalid.[48,49,54] The correlation time for, in particular, Leu13 deviates from the others, suggesting that the ^{15}N−^{1}H

Table 4. Overall Correlation Times (τ_{Mi}) and Squared Generalized Order Parameters (S^2) for the Six ^{15}N-Labeled Leu Residues in DPC and 9:1 DPC/DPG Micelles

	DPC micelles		9:1 DPC/DPG micelles	
residue	τ_{Mi} (ns)	S^2	τ_{Mi} (ns)[a]	S^2[b]
8	10.8 ± 1.8	0.71 ± 0.12	8.4 ± 1.4	0.97 ± 0.18
13	14.5 ± 1.8	0.65 ± 0.10	16.1 ± 1.4	–
15	11.1 ± 1.9	0.66 ± 0.12	8.1 ± 1.4	–
18	9.3 ± 1.3	0.85 ± 0.13	9.0 ± 1.8	0.97 ± 0.06
21	9.1 ± 1.3	0.83 ± 0.13	7.9 ± 0.4	0.96 ± 0.05
23	9.4 ± 1.4	0.80 ± 0.13	9.6 ± 2.0	0.91 ± 0.06

[a]Overall correlation times (τ_{Mi}) derived from fitting τ_M, S^2, and τ_{loc}. [b]Generalized order parameter squared derived using a τ_M of 8.0 ns and a model including S^2 and τ_{loc}.

dx.doi.org/10.1021/bi300188t | Biochemistry 2012, 51, 3982−3992

bond vector in Leu13 is modulated by a different motion due to anisotropic overall molecular motion, the presence of slow internal motion, or exchange. The latter is indeed indicated by the significantly faster R_2 relaxation (Figure 6). The average value for the correlation time, 10.7 ns, corresponds to a particle with a hydrodynamic radius of 23 Å, in agreement with estimates based on translational diffusion measurements of the peptide in DPC.[19] This corresponds to a volume of 50 nm^3, which can be identified by considering the paddle domain volume (estimated to be 4 nm^3) together with a somewhat larger DPC micelle.[19] Hence, the micelle aggregation number is slightly increased as compared to that without the peptide, which has also been seen for DPC micelles interacting with other peptides.[55] The fact that the overall correlation times agree well with the size of a peptide in a DPC micelle indicates that the analysis appears to be valid.

All six Leu residues have heteronuclear NOEs close to 1, i.e., very limited NOEs, indicating a well-defined rigid structure in the presence of DPC, which translates into relatively high order parameters (ranging between 0.65 and 0.85). Figure 5 shows the structure of HsapBKp in DPC with the Leu residues color-coded according to their order parameters in DPC. Leu18, Leu21, and Leu23, situated in the S4 helix, have order parameters that are relatively high (0.80−0.85). Leu8, situated in the S3b part of the sequence, has a significantly lower order parameter (0.71), and Leu13 and Leu15, in the hinge between the two helices, both have even lower S^2 values (0.65 and 0.66, respectively). The greater flexibility allowed for Leu13 and Leu15 suggests that this part of the domain may be responsible for the membrane perturbation by moving and hence breaking the tight seal between the surrounding lipids and the paddle domain. The τ_{loc} values were all long, between 1.1 and 3.1 ns, indicating, as indicated above, difficulties in correctly separating local and overall motion.

To investigate the effect of introducing negatively charged DPG into the micelles, relaxation for HsapBKp in 9:1 DPC/DPG micelles was measured (Figure 6, right panel). The sample aggregated over time, indicating a stronger interaction between the micelle and HsapBKp, which was also evident from increased line widths in the NMR spectra, and only R_1 and the NOE at 700 MHz and R_1 at 600 MHz were measured successfully. In addition, the relaxation parameters were more difficult to fit with the model-free approach. Nevertheless, by employing the same model that was used for the measurements in DPC, rotational correlation times on the same order of magnitude (with an average of 9.9 ns) were observed. The smaller overall correlation time compared to that in DPC is likely to be consequence of not having R_2 rates in the fit. Here, an even more striking difference between Leu13 and the other residues was observed (Table 4). Further, Leu8, Leu13, and Leu15 needed addition of an exchange term to produce a reasonable fit, but because of the lack of transverse relaxation parameters, this model was not used to estimate the overall rotational correlation time. Therefore, a fixed correlation time of 8 ns for the entire peptide was used, optimized on the basis of data for Leu8, Leu18, Leu21, and Leu23. Using this value, we obtained very high order parameters (0.91−0.97) for four residues (Leu8, Leu18, Leu21, and Leu23) using the same model, including S^2 and τ_{loc}. These high order parameters are at least partly likely to be a consequence of an unreasonably short overall correlation time, related to not having R_2 relaxation data in the fit. For Leu13 and Leu15, however, this procedure did not result in a usable fit. Together, this suggests that the interaction of the peptide with partly negatively charged micelles is different from the interaction with DPC micelles, leading to a dynamic behavior that is difficult to model from standard relaxation parameters using the model-free approach. Most likely, it involves slow motions with correlation times comparable to that of the overall rotation of the micelle, which makes the analysis fail.

In summary, the Leu residues located in the S4 segment, Leu18, Leu21, and Leu23, have overall correlation times close to the overall τ_M, suggesting a uniform motion of this part of the paddle domain in DPC. The S4 segment is rigid with S^2 parameters between 0.8 and 0.85 indicating that it is well-structured. However, significant internal motions on the nanosecond time scale are also present, possibly because of small conformational changes. The $^{15}N-^{1}H$ bond vectors in Leu13 and Leu15, situated in the turn of the helix−turn−helix motif close to the Trp residue, experience different overall motion, as indicated by differences in the estimated overall correlation times. This can be explained by anisotropic motion leading to different relaxation parameters in this part of the paddle domain and/or slow local motion that is impossible to separate from the overall motion. Also, the order parameters are lower for this part of the sequence, indicating more flexibility. When negative charge is introduced into the micelles, the dynamics of the turn is harder to fit, which further indicates the presence of slow local motions that are difficult to separate from overall motion. This is also evidenced by the markedly increased line widths in the spectra.

DISCUSSION

The combined results from observing membrane perturbation effects (from induced leakage from vesicles and effects on bilayer order), dynamics, and structure induction provide evidence for two main observations: the two paddles do not have the same effects on a bilayer, and the effects on the membrane depend on structural rearrangements and dynamics. The Arg-rich paddles from the KvAP and HsapBK potassium channels differ only slightly from each other with respect to hydrophobicity and the number of Arg residues, yet they are observed in this study to affect the membrane in different ways.

KvAPp is significantly α-helical in zwitterionic vesicles and is seen to cause a modest membrane perturbation at a P:L ratio of 1:20. Further, KvAPp increases the order of magnetically aligned bicelles, which suggests a well-defined peptide−lipid interaction, along the whole perdeuterated chain. Together, these results suggest that KvAPp is positioned as a transmembrane helix spanning the bilayer, which does not disrupt the membrane significantly. With an increase in the KvAPp concentration or upon addition of charged lipids to the vesicles, the amount of β-sheet is increased and also the effect on the membrane is strengthened. When KvAPp has a high β-sheet content together with a low α-helical content, the level of membrane perturbation increases with an increasing paddle domain concentration.

HsapBKp, on the other hand, is mainly β-structured at the concentrations used in the leakage studies and disrupts the membrane in a concentration-dependent manner. Because of the location of a Trp residue in the turn of the helix−turn−helix motif, HsapBKp is likely to be located at the water−lipid interface and might in this way be able to affect the membrane more than KvAPp is, which most likely is in a transmembrane position under these conditions. HsapBKp induces more calcein leakage in zwitterionic vesicles than in 30% negatively

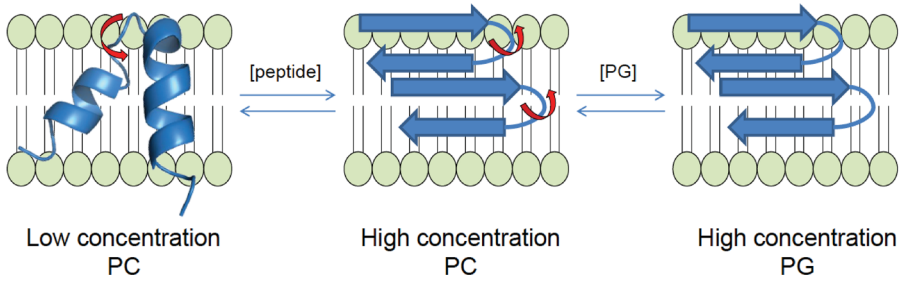

Figure 7. Model for how the HsapBKp paddle domain can undergo structural transitions, which affect the membrane perturbation. At low concentrations, the flexible turn in the largely α-helical peptide does not cause severe leakage from LUVs. Increasing the concentration causes the peptide to undergo a structural transition, which induces leakage. Upon addition of PG lipids to the bilayer, the structure is stabilized, and the dynamics are more restricted, which leads to a decrease in the level of leakage.

charged vesicles and, contrary to KvAPp, affects the morphology of magnetically aligned bicelles. Upon addition of DMPG to the magnetically aligned bilayers or with an increase in the paddle domain concentration, the change in morphology is more severe, hence indicating a different mode of interaction with zwitterionic and negatively charged bilayers. The binding to negatively charged bilayers is thus stronger, while the leakage is stronger in zwitterionic bilayers. Hence, a tighter binding of the peptide to the bilayer is correlated with less membrane perturbation.

Next, we turn to our second observation, that bilayer perturbations are correlated with dynamics. The analysis of relaxation data for HsapBKp showed that the turn in the helix−turn−helix motif is more dynamic than the rest of the motif. Further, the level of calcein leakage is seen to increase with increased flexibility in the turn region of the helix−turn−helix motif, which indicates that this part may be responsible for the bilayer perturbations. The turn is the part of the paddle domain that is most variable between channels,[3] and this may in part explain the difference in the degree of perturbation between the two paddle domains studied here. The well-structured S4 helix, on the other hand, is a strong candidate for being a spontaneous membrane-translocating peptide that does not cause perturbation.[56] The presence of a Trp residue in the turn region seems to increase the level of leakage significantly. Furthermore, we see that the S4 segment of HsapBKp is well-structured, but that the internal motions for all residues occur on a nanosecond time scale, which are likely to be due to structural transitions. Transitions between α-helical and 3_{10}-helical structures have previously been demonstrated for the S4 helix[9,57,58] and are suggested to be part of the gating mechanism. This small conformational change, where the α-helix becomes more tightly wound, is prolonged and thus becomes thinner, has been reported to occur on the order of nanoseconds.[59] Our previous structure of HsapBKp in DPC indicated both α-helical and 3_{10}-helical structure in the S4 segment supporting such a structural transition.[19] We believe that these observations suggest that paddle domains appear to be able to undergo structural transitions and have enhanced flexibility in the turn and that there is a correlation between these properties and membrane perturbing effects. Together, this provides a possible mechanism for how the paddle moves in a bilayer. A model for how this bilayer perturbation occurs as a consequence of an increase in the paddle domain concentration and of negatively charged lipids is shown in Figure 7.

The sequence properties of paddle motifs are shared with several biologically active peptides, such as antimicrobial peptides, and cell-penetrating peptides. The calcein leakage induced by KvAPp and HsapBKp was compared with that in previous studies performed for peptides found to function as CPPs: M918,[34] mPrPp, and bPrPp.[35] M918 is less hydrophobic than both paddle domains but has more Arg residues. In previous studies, M918 has been shown to induce a modest amount of leakage from both types of vesicles.[23,34] The prion protein-derived peptides, mPrPp and bPrPp, induce more leakage, comparable to the leakage induced by HsapBKp.[35] These sequences are less hydrophobic than the paddle domains but have a similar net charge (in this case Lys). Further, mPrPp and bPrPp have significant β-sheet content, and the level of induced leakage increases with elevated β-sheet content. The β-sheet content is as for KvAPp increased upon addition of charge to the vesicle.[35] The prion protein-derived peptides contain a Trp residue, and it has previously been seen that Trp content might be related to an increase in the level of leakage.[60] In summary, a certain amount of β-sheet content together with Trp content, locating the peptide at the water−lipid interface, may be important factors related to membrane perturbation. Our data, together with previous work, show that the amount of leakage can generally not be predicted from the Arg (or Lys) content and hydrophobicity alone, even though basic residues and hydrophobicity seem to be necessary for leakage to occur in LUV model systems.

Finally, one can also draw a conclusion about the two paddle domains as parts of the VSD in potassium channels. It has been shown experimentally and in MD simulations that the VSD induces a thinning of a bilayer,[9,61−64] which may be a significant part of the gating mechanism. Studies have shown that the S4 helix alone also induces a thinning of the membrane, similar to what is observed for the VSD.[11,17,65] A thinning mechanism is likely to be related to a more general membrane perturbation, as observed here. Some time ago,[22] we suggested a model in which leakage was induced by a transient rearrangement of a peptide in a bilayer, which gives rise to a graded leakage as in the study presented here. The induction of leakage by the isolated Arg-rich paddle domains observed in our study may thus in fact be correlated with a more general thinning effect produced by the whole VSD. Our results demonstrate that the perturbation is caused by the dynamic region in the paddle. They also indicate that the dynamics are likely to be related to structural transitions, which may also be important for the gating mechanism. The thinning effect would then be compatible with a gating mechanism in which a movement of the whole paddle domain does not need to be that large.

dx.doi.org/10.1021/bi300188t | *Biochemistry* 2012, 51, 3982−3992

AUTHOR INFORMATION

Corresponding Author

*E-mail: lena.maler@dbb.su.se. Phone: +46 8 162448. Fax: +46 8 155597.

Funding

This work was supported by grants from the Swedish Research Council and the Carl Trygger Foundation.

Notes

The authors declare no competing financial interest.

ABBREVIATIONS

K_v channel, voltage-gated K^+ channel; VSD, voltage-sensing domain; CPP, cell-penetrating peptide; P:L ratio, peptide:lipid ratio; LUV, large unilamellar vesicle; KvAP, *A. pernix* K^+ channel; HsapBK, *H. sapiens* BK K^+ channel; CD, circular dichroism; NMR, nuclear magnetic resonance; DMPC, 1,2-dimyristoyl-*sn*-glycero-3-phosphocholine; DMPG, 1,2-dimyristoyl-*sn*-glycero-3-phospho-(1′-*rac*-glycerol); DPC, dodecylphosphocholine; DPG, dodecylphospho-*rac*-glycerol sodium salt; POPC, 1-palmitoyl-2-oleoyl-*sn*-glycero-3-phosphocholine; POPG, 1-palmitoyl-2-oleoyl-*sn*-glycero-3-phospho-(1′-*rac*-glycerol); DHPC, 1,2-dihexanoyl-d_{22}-*sn*-glycero-3-phosphocholine; $\Delta\nu_q$, quadrupolar splitting; S_{CD}, order parameter; T_1, longitudinal relaxation time; T_2, transverse relaxation time; NOE, nuclear Overhauser effect; S^2, generalized order parameter; MD, molecular dynamics.

REFERENCES

(1) Bezanilla, F. (2000) The Voltage Sensor in Voltage-Dependent Ion Channels. *Physiol. Rev. 80*, 555−592.

(2) Jiang, Y., Ruta, V., Chen, J., Lee, A., and MacKinnon, R. (2003) The Principle of Gating Charge Movement in a Voltage-Dependent K^+ Channel. *Nature 423*, 42−48.

(3) Jiang, Y., Lee, A., Chen, J., Ruta, V., Cadene, M., Chait, B. T., and MacKinnon, R. (2003) X-ray Structure of a Voltage-Dependent K^+ Channel. *Nature 423*, 33−41.

(4) Lee, S. Y., Lee, A., Chen, J., and MacKinnon, R. (2005) Structure of the KvAP Voltage-Dependent K^+ Channel and its Dependence on the Lipid Membrane. *Proc. Natl. Acad. Sci. U.S.A. 102*, 15441−15446.

(5) Posson, D. J., Ge, P., Miller, C., Bezanilla, F., and Selvin, P. R. (2005) Small Vertical Movement of a K^+ Channel Voltage Sensor Measured with Luminescence Energy Transfer. *Nature 436*, 848−851.

(6) Cuello, L. G., Cortes, D. M., and Perozo, E. (2004) Molecular Architecture of the KvAP Voltage-Dependent K^+ Channel in a Lipid Bilayer. *Science 306*, 491−495.

(7) Hristova, K., and Wimley, W. C. (2011) A look at arginine in membranes. *J. Membr. Biol. 239*, 49−56.

(8) Andersen, O. S., and Koeppe, R. E. (2007) Bilayer Thickness and Membrane Protein Function: An Energetic Perspective. *Annu. Rev. Biophys. Biomol. Struct. 36*, 107−130.

(9) Bjelkmar, P., Niemelä, P. S., Vattulainen, I., and Lindahl, E. (2009) Conformational Changes and Slow Dynamics through Microsecond Polarized Atomistic Molecular Simulation of an Integral Kv1.2 Ion Channel. *PLoS Comput. Biol. 5*, e1000289.

(10) Schow, E. V., Freites, J. A., Cheng, P., Bernsel, A., von Heijne, G., White, S. H., and Tobias, D. J. (2011) Arginine in Membranes: The Connection between Molecular Dynamics Simulations and Translocon-Mediated Insertion Experiments. *J. Membr. Biol. 239*, 35−48.

(11) Doherty, T., Su, Y., and Hong, M. (2010) High-resolution orientation and depth of insertion of the voltage-sensing S4 helix of a potassium channel in lipid bilayers. *J. Mol. Biol. 401*, 642−652.

(12) Ramsey, I. S., Moran, M. M., Chong, J. A., and Clapham, D. E. (2006) A voltage-gated proton-selective channel lacking the pore domain. *Nature 440*, 1213−1216.

(13) Sasaki, M., Takagi, M., and Okamura, Y. (2006) A voltage sensor-domain protein is a voltage-gated proton channel. *Science 312*, 589−592.

(14) Alabi, A. A., Bahamonde, M. I., Jung, H. J., Kim, J. I., and Swartz, K. J. (2007) Portability of paddle motif function and pharmacology in voltage sensors. *Nature 450*, 370−375.

(15) Bosmans, F., Martin-Euclaire, M.-F., and Swartz, K. J. (2008) Deconstructing voltage sensor function and pharmacology in sodium channels. *Nature 456*, 202−208.

(16) Swartz, K. J. (2008) Sensing voltage across lipid membranes. *Nature 456*, 891−897.

(17) Hong, M., and Su, Y. (2011) Structure and dynamics of cationic membrane peptides and proteins: Insights from solid-state NMR. *Protein Sci. 20*, 641−655.

(18) Freites, J. A., Tobias, D. J., Von Heijne, G., and White, S. H. (2005) Interface Connections of a Transmembrane Voltage Sensor. *Proc. Natl. Acad. Sci. U.S.A. 102*, 15059−15064.

(19) Unnerståle, S., Lind, J., Papadopoulos, E., and Mäler, L. (2009) Solution Structure of the HsapBK K Channel Voltage-Sensor Paddle Sequence. *Biochemistry 48*, 5813−5821.

(20) Chen, R. F., and Knutson, J. R. (1988) Mechanism of Fluorescence Concentration Quenching of Carboxyfluorescein in Liposomes: Energy Transfer to Nonfluorescent Dimers. *Anal. Biochem. 172*, 61−77.

(21) Arbuzova, A., and Schwarz, G. (1999) Pore-Forming Action of Mastoparan Peptides on Liposomes: A Quantitative Analysis. *Biochim. Biophys. Acta 1420*, 139−152.

(22) Andersson, A., Danielsson, J., Gräslund, A., and Mäler, L. (2007) Kinetic Models for Peptide-Induced Leakage from Vesicles and Cells. *Eur. Biophys. J. 36*, 621−635.

(23) Guterstam, P., Madani, F., Hirose, H., Takeuchi, T., Futaki, S., el Andaloussi, S., Graslund, A., and Langel, U. (2009) Elucidating Cell-Penetrating Peptide Mechanisms of Action for Membrane Interaction, Cellular Uptake, and Translocation Utilizing the Hydrophobic Counter-Anion Pyrenebutyrate. *Biochim. Biophys. Acta 1788*, 2509−2517.

(24) Futaki, S., Suzuki, T., Ohashi, W., Yagami, T., Tanaka, S., Ueda, K., and Sugiura, Y. (2001) Arginine-Rich Peptides. *J. Biol. Chem. 276*, 5836−5840.

(25) Jarver, P., and Langel, U. (2006) Cell-Penetrating Peptides: A Brief Introduction. *Biochim. Biophys. Acta 1758*, 260−263.

(26) Dempsey, C. E. (1990) The Actions of Melittin on Membranes. *Biochim. Biophys. Acta 1031*, 143−161.

(27) Habermann, E. (1972) Bee and Wasp Venoms. *Science 177*, 314−322.

(28) Yeaman, M. R., and Yount, N. Y. (2003) Mechanisms of Antimicrobial Peptide Action and Resistance. *Pharmacol. Rev. 55*, 27−55.

(29) Papagianni, M. (2003) Ribosomally Synthesized Peptides with Antimicrobial Properties: Biosynthesis, Structure, Function, and Applications. *Biotechnol. Adv. 21*, 465−499.

(30) Wildman, K. A. H., Lee, D. K., and Ramamoorthy, A. (2003) Mechanism of Lipid Bilayer Disruption by the Human Antimicrobial Peptide, LL-37. *Biochemistry 42*, 6545−6558.

(31) Wimley, W. C., and Hristova, K. (2011) Antimicrobial Peptides: Successes, Challenges and Unanswered Questions. *J. Membr. Biol. 239*, 27−34.

(32) Madani, F., Lindberg, S., Langel, U., Futaki, S., and Gräslund, A. (2011) Mechanisms of Cellular Uptake of Cell-Penetrating Peptides. *J. Biophys. 2011*, 1−9.

(33) Lindgren, M., Hallbrink, M., Prochiantz, A., and Langel, U. (2000) Cell-Penetrating Peptides. *Trends Pharmacol. Sci. 21*, 99−103.

(34) El-Andaloussi, S., Johansson, H. J., Holm, T., and Langel, Ü. (2007) A Novel Cell-Penetrating Peptide, M918, for Efficient Delivery of Proteins and Peptide Nucleic Acids. *Mol. Ther. 15*, 1820−1826.

(35) Magzoub, M., Oglecka, K., Pramanik, A., Goran Eriksson, L., and Graslund, A. (2005) Membrane Perturbation Effects of Peptides Derived from the N-Termini of Unprocessed Prion Proteins. *Biochim. Biophys. Acta 1716*, 126−136.

(36) Mayer, L., Hope, M., and Cullis, P. (1986) Vesicles of Variable Sizes Produced by a Rapid Extrusion Procedure. *Biochim. Biophys. Acta 858*, 161−168.
(37) Compton, L. A., and Johnson, W. C. (1986) Analysis of Protein Circular Dichroism Spectra for Secondary Structure using a Simple Matrix Multiplication. *Anal. Biochem. 155*, 155−167.
(38) Manavalan, P., and Johnson, W. C. (1987) Variable Selection Method Improves the Prediction of Protein Secondary Structure from Circular Dichroism Spectra. *Anal. Biochem. 167*, 76−85.
(39) Sreerama, N., and Woody, R. W. (2000) Estimation of Protein Secondary Structure from Circular Dichroism Spectra: Comparison of CONTIN, SELCON, and CDSSTR Methods with an Expanded Reference Set. *Anal. Biochem. 287*, 252−260.
(40) Lobley, A., Whitmore, L., and Wallace, B. A. (2002) DICHROWEB: An Interactive Website for the Analysis of Protein Secondary Structure from Circular Dichroism Spectra. *Bioinformatics 18*, 211−212.
(41) Aussenac, F., Laguerre, M., Schmitter, J. M., and Dufourc, E. J. (2003) Detailed Structure and Dynamics of Bicelle Phospholipids using Selectively Deuterated and Perdeuterated Labels. ^{2}H NMR and Molecular Mechanics Study. *Langmuir 19*, 10468−10479.
(42) Burnett, L., and Muller, B. (1971) Deuteron Quadrupole Coupling Constants in Three Solid Deuterated Paraffin Hydrocarbons: C_2D_6, C_4D_{10}, C_6D_{14}. *J. Chem. Phys. 55*, 5829−5831.
(43) de Planque, M. R. R., Greathouse, D. V., Koeppe, R. E., II, Schäfer, H., Marsh, D., and Killian, J. A. (1998) Influence of lipid/peptide Hydrophobic Mismatch on the Thickness of Diacylphosphatidylcholine Bilayers. A ^{2}H NMR and ESR Study using Designed Transmembrane α-Helical Peptides and Gramicidin A. *Biochemistry 37*, 9333−9345.
(44) Kay, L., Keifer, P., and Saarinen, T. (1992) Pure Absorption Gradient Enhanced Heteronuclear Single Quantum Correlation Spectroscopy with Improved Sensitivity. *J. Am. Chem. Soc. 114*, 10663−10665.
(45) Skelton, N., Palmer, A., Akke, M., Kordel, J., Rance, M., and Chazin, W. (1993) Practical Aspects of Two-Dimensional Proton-Detected ^{15}N Spin Relaxation Measurements. *J. Magn. Reson., Ser. B 102*, 253−264.
(46) Mandel, A. M., Akke, M., and Palmer, A. G. (1995) Backbone Dynamics of *Escherichia coli* Ribonuclease HI: Correlations with Structure and Function in an Active Enzyme. *J. Mol. Biol. 246*, 144−163.
(47) Palmer, A. G. (1991) Sensitivity Improvement in Proton-Detected Two-Dimensional Heteronuclear Correlation NMR Spectroscopy. *J. Magn. Reson. 93*, 151−170.
(48) Lipari, G., and Szabo, A. (1982) Model-Free Approach to the Interpretation of Nuclear Magnetic Resonance Relaxation in Macromolecules. 1. Theory and Range of Validity. *J. Am. Chem. Soc. 104*, 4546−4559.
(49) Lipari, G., and Szabo, A. (1982) Model-Free Approach to the Interpretation of Nuclear Magnetic Resonance Relaxation in Macromolecules. 2. Analysis of Experimental Results. *J. Am. Chem. Soc. 104*, 4559−4570.
(50) Salsbury, N., Darke, A., and Chapman, D. (1972) Deuteron Magnetic Resonance Studies of Water Associated with Phospholipids. *Chem. Phys. Lipids 8*, 142−151.
(51) Finer, E., and Darke, A. (1974) Phospholipid Hydration Studied by Deuteron Magnetic Resonance Spectroscopy. *Chem. Phys. Lipids 12*, 1−16.
(52) Biverståhl, H., Lind, J., Bodor, A., and Mäler, L. (2009) Biophysical Studies of the Membrane Location of the Voltage-Gated Sensors in the HsapBK and KvAP K^+ Channels. *Biochim. Biophys. Acta 1788*, 1976−1986.
(53) Schleucher, J., Schwendinger, M., Sattler, M., Schmidt, P., Schedletzky, O., Glaser, S. J., Sørensen, O. W., and Griesinger, C. (1994) A General Enhancement Scheme in Heteronuclear Multidimensional NMR Employing Pulsed Field Gradients. *J. Biomol. NMR 4*, 301−306.
(54) Kowalewski, J., and Mäler, L. (2006) *Nuclear spin relaxation in liquids: Theory, experiments, and applications*, Taylor & Francis, New York.
(55) Beswick, V., Guerois, R., Cordier-Ochsenbein, F., Coïc, Y. M., Huynh-Dinh, T., Tostain, J., Noël, J. P., Sanson, A., and Neumann, J. M. (1998) Dodecylphosphocholine Micelles as a Membrane-Like Environment: New Results from NMR Relaxation and Paramagnetic Relaxation Enhancement Analysis. *Eur. Biophys. J. 28*, 48−58.
(56) Marks, J. R., Palcone, J., Hristova, K., and Wimley, W. C. (2011) Spontaneous Membrane-Translocating Peptides by Orthogonal High-Throughput Screening. *J. Am. Chem. Soc. 133*, 8995−9004.
(57) Long, S. B., Tao, X., Campbell, E. B., and MacKinnon, R. (2007) Atomic Structure of a Voltage-Dependent K^+ Channel in a Lipid Membrane-Like Environment. *Nature 450*, 376−382.
(58) Villalba-Galea, C. A., Sandtner, W., Starace, D. M., and Bezanilla, F. (2008) S4-Based Voltage Sensors have Three Major Conformations. *Proc. Natl. Acad. Sci. U.S.A. 105*, 17600−17607.
(59) Vieira-Pires, R. S., and Morais-Cabral, J. H. (2010) 3_{10} Helices in Channels and Other Membrane Proteins. *J. Gen. Physiol. 136*, 585.
(60) Madani, F., Taqi, M. M., Wärmländer, S. K. T. S., Verbeek, D. S., Bakalkin, G., and Gräslund, A. (2011) Perturbations of Model Membranes Induced by Pathogenic Dynorphin A Mutants Causing Neurodegeneration in Human Brain. *Biochem. Biophys. Res. Commun. 411*, 111−114.
(61) Freites, J. A., Tobias, D. J., and White, S. H. (2006) A Voltage-Sensor Water Pore. *Biophys. J. 91*, L90−L92.
(62) Jogini, V., and Roux, B. (2007) Dynamics of the Kv1.2 Voltage-Gated K^+ Channel in a Membrane Environment. *Biophys. J. 93*, 3070−3082.
(63) Sands, Z. A., and Sansom, M. S. P. (2007) How does a Voltage Sensor Interact with a Lipid Bilayer? Simulations of a Potassium Channel Domain. *Structure 15*, 235−244.
(64) Krepkiy, D., Mihailescu, M., Freites, J. A., Schow, E. V., Worcester, D. L., Gawrisch, K., Tobias, D. J., White, S. H., and Swartz, K. J. (2009) Structure and Hydration of Membranes Embedded with Voltage-Sensing Domains. *Nature 462*, 473−479.
(65) Hessa, T., Kim, H., Bihlmaier, K., Lundin, C., Boekel, J., Andersson, H., Nilsson, I. M., White, S. H., and Von Heijne, G. (2005) Recognition of Transmembrane Helices by the Endoplasmic Reticulum Translocon. *Nature 433*, 377−381.